

# UCLA

## UCLA Previously Published Works

### Title

Response to Programmed Cell Death-1 Blockade in a Murine Melanoma Syngeneic Model Requires Costimulation, CD4, and CD8 T Cells.

### Permalink

<https://escholarship.org/uc/item/5kr4r168>

### Journal

Cancer immunology research, 4(10)

### ISSN

2326-6066

### Authors

Homet Moreno, Blanca  
Zaretsky, Jesse M  
Garcia-Diaz, Angel  
[et al.](#)

### Publication Date

2016-10-01

### DOI

10.1158/2326-6066.cir-16-0060

Peer reviewed

1  
2 Q1 **Response to Programmed Cell Death-1 Blockade**  
3 Q2 **in a Murine Melanoma Syngeneic Model Requires**  
4 **Costimulation, CD4, and CD8 T Cells**

5 AU Blanca Homet Moreno<sup>1</sup>, Jesse M. Zaretsky<sup>1,2</sup>, Angel Garcia-Diaz<sup>1</sup>, Jennifer Tsoi<sup>2</sup>,  
6 Giulia Parisi<sup>1</sup>, Lidia Robert<sup>1</sup>, Katrina Meeth<sup>3,4</sup>, Abibatou Ndoeye<sup>5</sup>, Marcus Bosenberg<sup>3,4</sup>,  
7 Ashani T. Weeraratna<sup>5</sup>, Thomas G. Graeber<sup>2,6</sup>, Begoña Comin-Anduix<sup>6,7</sup>,  
8 Siwen Hu-Lieskovan<sup>1,6</sup>, and Antoni Ribas<sup>1,2,6,7</sup>

9 **Abstract**

10 The programmed cell death protein 1 (PD-1) limits effector  
11 T-cell functions in peripheral tissues, and its inhibition leads  
12 to clinical benefit in different cancers. To better understand how  
13 PD-1 blockade therapy modulates the tumor–host interactions,  
14 we evaluated three syngeneic murine tumor models, the  
15 *BRAF*<sup>V600E</sup>-driven YUMM1.1 and YUMM2.1 melanomas, and  
16 the carcinogen-induced murine colon adenocarcinoma  
17 MC38. The YUMM cell lines were established from mice with  
18 melanocyte-specific *BRAF*<sup>V600E</sup> mutation and *PTEN* loss  
19 (*BRAF*<sup>V600E</sup>/*PTEN*<sup>-/-</sup>). Anti-PD-1 or anti-PD-L1 therapy engen-  
20 dered strong antitumor activity against MC38 and YUMM2.1, but  
21 not YUMM1.1. PD-L1 expression did not differ between the three  
22 models at baseline or upon interferon stimulation. Whereas

mutational load was high in MC38, it was lower in both YUMM  
models. In YUMM2.1, the antitumor activity of PD-1 blockade  
had a critical requirement for both CD4 and CD8 T cells, as well as  
CD28 and CD80/86 costimulation, with an increase in CD11c<sup>+</sup>  
CD11b<sup>+</sup>MHC-II<sup>high</sup> dendritic cells and tumor-associated macro-  
phages in the tumors after PD-1 blockade. Compared with  
YUMM1.1, YUMM2.1 exhibited a more inflammatory profile by  
RNA sequencing analysis, with an increase in expression from  
chemokine-trafficking genes that are related to immune cell  
recruitment and T-cell priming. In conclusion, response to PD-  
1 blockade therapy in tumor models requires CD4 and CD8 T cells  
and costimulation that is mediated by dendritic cells and macro-  
phages. *Cancer Immunol Res*; 4(10); 1–13. ©2016 AACR.

38 **Introduction**

39 The development of inhibitors of the programmed cell death  
40 protein 1 (PD-1) or its ligand (PD-L1) represents a paradigm shift  
41 in the treatment of advanced cancers, with significant clinical  
42 benefits demonstrated in patients with several different histologi-  
43 es (1–4). Tumor responses are associated with a higher number  
44 of pretreatment PD-L1–expressing tumor and myeloid cells (5, 6),  
45 a high mutational load leading to increase in antigen-specific

T-cell recognition (7, 8), the ability of PD-1/PD-L1 blockade to  
increase antigen presentation (9, 10) and modulate the tumor  
microenvironment (10, 11), and pre-existing CD8 T-cell infiltra-  
tion (5, 12). A higher tumor mutational load induced by carcino-  
gens such as ultraviolet light for melanoma (13) or cigarette  
smoking for lung carcinomas (14) would allow T cells to better  
differentiate between cancer and normal cells, thereby leading to  
immune recognition that could be unleashed by PD-1 blockade  
therapy.

Despite these advances, a better understanding is needed of the  
tumor–host interactions and how anti-PD-1 agents modulate  
cellular and molecular characteristics of each individual micro-  
environment. It is widely accepted that PD-1 blockade agents  
regulate T-cell activity in peripheral tissues in the context of  
infection or in tumors where PD-1/L1 checkpoint is the dominant  
inhibitory pathway. However, anti-PD-1 interacts earlier with T  
cells positively regulated by B7-CD28 costimulation (15), and  
this interaction is less well characterized (16–18).

In this study, we analyzed different tumor–host characteristics  
that might influence the effects of PD-1 blockade in murine models  
with a fully functional immune system. We conclude that T-cell  
priming and costimulation are required for anti-PD-1 therapy  
response to be effective in the melanoma tumor models *in vivo*.

**Materials and Methods**

**Mice, cell lines, and reagents**

C57BL/6 mice, B6.Cg-BraTm1MmcmPtentm1HwuTg(Tyr-cre/  
ERT2)13Bos/BosJ, B6.129S2-Cd28tm1Mak/J, and B6.129S4-

Q3 <sup>1</sup>Division of Hematology/Oncology, Department of Medicine, Univer-  
sity of California (UCLA), Los Angeles, California. <sup>2</sup>Department of  
Molecular and Medical Pharmacology, UCLA, Los Angeles, California.  
Q4 <sup>3</sup>Departments of Immunobiology, Dermatology, and Pathology, Yale  
University School of Medicine, New Haven, Connecticut. <sup>4</sup>Howard  
Hughes Medical Institute, Chevy Chase, Maryland. <sup>5</sup>Melanoma  
Research Center, The Wistar Institute, Philadelphia, Pennsylvania.  
<sup>6</sup>Jonsson Comprehensive Cancer Center (JCCC) at UCLA, Los  
Angeles, California. <sup>7</sup>Division of Surgical Oncology, Department of  
Surgery, UCLA, Los Angeles, California.

**Note:** Supplementary data for this article are available at Cancer Immunology  
Research Online (<http://cancerimmunolres.aacrjournals.org/>).

Q5 **Corresponding Authors:** A. Ribas, University of California, Los Angeles, 10833 Le  
Conte Avenue, Los Angeles, CA 90095. Phone: 310-206-3928; Fax: 310-825-  
2493; E-mail: aribas@mednet.ucla.edu; or S. Hu-Lieskovan, Division of Hema-  
tology-Oncology, 11-934 Factor Building, 10833 Le Conte Avenue, Los Angeles,  
CA 90095-1782. Phone: 310-794-4955; Fax: 310-825-2493; E-mail:  
shu-lieskovan@mednet.ucla.edu

**doi:** 10.1158/2326-6066.CIR-16-0060

©2016 American Association for Cancer Research.

76	Cd80tm1Shr Cd86tm2Shr/J mice (Jackson Laboratories) were	136
77	bred and kept under defined-flora pathogen-free conditions at	137
78 Q6	the AALAC-approved animal facility of the Division of Experi-	138
79	mental Radiation Oncology, UCLA, and used under the UCLA	139
80	Animal Research Committee protocol #2004-159-23. Cell lines	140
81	were cultured in DMEM media (Invitrogen) supplemented with	141
82	10% FBS (Omega Scientific) and 2 nmol/L L-glutamine (Invitro-	142
83 Q7	gen). YUMM1.1 and YUMM1.7 cell lines were obtained from	143
84	induced tumors in conditional mouse models of melanoma	144
85	based on melanocyte-specific <i>BRAF</i> <sup>V600E</sup> activating mutation and	Q8 145
86	<i>PTEN</i> loss ( <i>BRAF</i> <sup>V600E</sup> / <i>PTEN</i> <sup>-/-</sup> ). YUMM2.1 was obtained from	
87	<i>BRAF</i> <sup>V600E</sup> / <i>PTEN</i> <sup>-/-</sup> mice crossed with mice bearing a <i>Ctnnb1</i> <sup>loxex3</sup>	
88	allele (19), which targets exon 3, resulting in removal of the	
89	GSK3b kinase sites in β-catenin that are needed for ubiquitin-	
90	mediated destruction. However, analysis of the YUMM2.1 cell	
91	line showed that it had not recombined the β-catenin site (see	
92	below). YUMM cell lines were tested and authenticated by PCR	
93	and exome sequencing. Recombinant murine interferon gamma	
94	(IFNγ) was obtained from Peprotech. Tumors were followed by	
95	caliper measurement three times per week, and tumor volume was	
96	calculated using the following formula: tumor volume =	
97	((width) <sup>2</sup> × length)/2. Mean and SD of the tumor volumes per	
98	group were calculated.	
99	<b>Antitumor studies in mouse models</b>	
100	To establish subcutaneous (s.c.) tumors, 3 × 10 <sup>5</sup> MC38, 1 × 10 <sup>6</sup>	
101	YUMM2.1, or 1 × 10 <sup>6</sup> YUMM1.1 cells per mouse were injected	
102	into the flanks of C57BL/6 mice. When tumor diameter reached 4	
103	to 5 mm, four doses of 300 μg of anti-PD-1 (Cat. No. BE0146,	
104	clone RMP1-14), anti-PD-L1 (Cat. No. BE0101, clone 10F.9G2),	
105	or isotype control antibody (Cat. No. BE0090, clone LTF-2), all	
106	from BioXCell, were injected intraperitoneally (i.p.) every 3 days.	
107	For T-cell subset depletion studies, 250 μg of anti-CD8 (Cat. No.	
108	BE0117, clone YTS 169.4), 250 μg of anti-CD4 (Cat. No. BE0003-	
109	2, clone OKT-4), both from BioXCell, or the combination were	
110	administered every 2 days starting the day before anti-PD-1 was	
111	initiated and through the duration of the experiment. For CD103	
112	depletion, 200 μg of CD103 (Cat. No. BE0026, clone M290) from	
113	BioXCell was administered starting the day before anti-PD-1	
114	treatment was initiated and administered i.p. every 2 days until	
115	the end of the experiment.	
116	<b>Whole-exome sequencing: Mutation calling and copy-number</b>	
117	<b>analysis</b>	
118	Sequencing of the MC38, YUMM2.1, YUMM1.7, and	
119	YUMM1.1 cell lines was performed to a mean depth of	
120	55X, with >90% of targeted bases covered by more than 15	
121	reads in all samples. Exonic mutations were annotated by the	
122	Ensembl Variant Effect Predictor (EVEP). MC38 was compared	
123	with tail DNA from a C57BL6 parental mouse, whereas the	
124	YUMM2.1 and YUMM1.1 were compared with tail DNA	
125	from a B6.Cg-Bra <sup>tm1MmcmPtentm1HwiTg</sup> (Tyr-cre/ERT2)	
126	13Bos/BosJ mouse. Exon capture and library preparation were	
127	performed at the UCLA Clinical Microarray Core using the	
128	NimbleGenSeqCap EZ Mouse Exome Design Kit (Roche Nim-	
129	bleGen) targeting 54.3 megabases of genome. Note that 2 ×	
130	100 bp paired-end sequencing was carried out on the HiSeq	
131	2000 platform (Illumina), and sequences were aligned to the	
132	UCSC mm10 reference (Burrows-Wheeler Aligner BWA-mem	
133	algorithm v0.7.9). Preprocessing followed the Genome Anal-	
134	ysis Toolkit (GATK) Best Practices Workflow v3 (20), including	
	duplicate removal (Picard), indel realignment, and base qual-	136
	ity score recalibration. Somatic mutations were called with	137
	methods modified from ref. 21 using Varscan2 (22), and the	138
	GATK-HaplotypeCaller. Mutations were annotated by EVEP	139
	release 80 (23) and filtered to remove those with a known	140
	database single-nucleotide polymorphism (dbSNP) reference	141
	SNP cluster identification to exclude residual strain-related	142
	differences due to imperfect backcross dilution. Depth ratio	143
	for copy-number variation was produced by Sequenza (24),	144
	with the ratio.priority option engaged.	Q8 145
	<b>RNA sequencing and enrichment analysis</b>	146
	RNA sequencing was performed using the Illumina HiSeq 2500	147
	platform on 100-bp paired-end libraries prepared using the	148
	IlluminaTruSeq RNA sample preparation Kit. Reads were mapped	149
	using TopHat2 v2.0.9 (25) and aligned to the Mus musculus	150
	genome NCBI build 37.2. Reads were quantified and normalized	151
	using Cufflinks v2.2.1 (26) and CuffNorm to generate normalized	152
	expression tables by library size using the geometric normaliza-	153
	tion method. Resulting fragments per kilobase of exon per million	154
	fragments mapped expression values were log <sub>2</sub> transformed with	155
	an offset of 1. To identify pathways enriched in the YUMM2.1 cell	156
	line, Gene Set Enrichment Analysis (GSEA) was performed using	157
	the preranked option. Genes were ranked by log <sub>2</sub> fold changes	158
	between YUMM2.1 and YUMM1.1 cell lines. Enrichment was	159
	assessed across the curated Molecular Signatures Database C5 GO	160
	biological process gene sets (27). RNA sequencing data have been	161
	deposited in GEO repository under the accession number	162
	GSE84264.	163
	<b>Flow cytometry analysis</b>	164
	MC38, YUMM2.1, and YUMM1.1 tumors and spleens were	165
	harvested from mice at predefined time points. Tumors were	166
	digested with collagenase D (Roche) and stained with antibodies	167
	to CD3 BV605, Ly6C FITC, PD-L1/CD274 PE, CD8a BV421,	168
	CD45RA/B220, CD11b BV785, CD11c PECy7, CD103 PerCP	169
	Cyanine 5.5, MHC Class II (I-A/I-E) FITC (Biolegend), Ly6G	170
	(Gr-1) PerCP Cyanine 5.5, F4/80 Pacific blue/eFluor450, CD25	171
	APC, CD4 FITC (eBioscience). Intracellular staining of Foxp3 PE	172
	(eBioscience) was done according to the manufacturer's recom-	173
	mendations. Cells were analyzed with a LSR-II or FACSCalibur	174
	flow cytometer (BD Biosciences), followed by Flow-Jo software	175
	(Tree-Star) analysis (28).	176
	<b>Western blotting and immunofluorescence staining</b>	177
	Western blotting was performed using standard methods on	178
	lysates from cultured murine melanoma cell lines using	179
	primary antibodies to β-catenin, GAPDH and histone H3,	180
	and secondary anti-rabbit IgG horseradish peroxidase-linked	181
	antibody, all from Cell Signaling Technology, and Pdc <sup>d</sup> -1L1	182
	(H-130) and gp100 (H-300) from Santa Cruz Biotechnology.	183
	Nuclear and cytoplasmic extraction reagents were obtained	184
	from Thermo Scientific. Proteins were visualized using Im-	185
	ageQuant 4000 scanner. Immunofluorescence staining was	186
	performed on tumor sections of frozen OCT blocks (Sakura	Q9 187
	Finetek) using primary antibodies to β-catenin (Cell Signaling	188
	Technology) and CD8a (BD Biosciences) followed by	189
	normal donkey serum and rat IgG(H+L) FITC-conjugated	190
	secondary antibody (Jackson Immunoresearch Laboratories;	191
	ref. 29).	192

### 195 Topflash analysis

196 Topflash vectors were obtained from Addgene (M51 Super 8x  
197 FOPFlash/TOPFlash mutant, Cat. No. 12457; M50 Super 8x  
198 TOPFlash, Cat. No. 12456). YUMM1.7 and YUMM2.1 cells  
199 ( $\pm 10 \mu\text{mol/L}$  tamoxifen) were plated to achieve 70% confluency  
200 in 6-well plates. Cells were cotransfected with pTK-RLuc (green  
201 Renilla luciferase) along with either Topflash or Fopflash vectors.  
202 After 48 hours, cells were harvested and luciferase activity was  
203 measured using Dual-Luciferase Reporter Assay System (Cat. No.  
204 E1910) from Promega, where firefly luciferase signal was normal-  
205 ized to its corresponding Renilla luciferase signal. Topflash/fop-  
206 flash signal was determined from each treatment and graphed  
207 using Graphpad/Prism.

### 208 $\beta$ -Catenin downregulation

209  $\beta$ -catenin shRNA lentiviral vector (Cat. No. 29210-V) and the  
210 negative control shRNA lentiviral vector (Cat. No. 108080) were  
211 purchased from Santa Cruz Biotechnology. YUMM2.1 and  
212 YUMM1.1 cells were transduced at a multiplicity of infection of  
213 1 to 10 in media containing  $5 \mu\text{g/mL}$  polybrene and then selected  
214 in complete DMEM with  $2.5 \mu\text{g/mL}$  of puromycin for 3 weeks.

### 215 Statistical analysis

216 Data were analyzed with GraphPad Prism (version 5) software  
217 (GraphPad Software). Descriptive statistics such as number of  
218 observations, mean values, and SD were reported and presented  
219 graphically for quantitative measurements. Normality assump-  
220 tion was checked for outcomes before statistical testing. For  
221 measurements such as tumor volume or percentage of tumor-  
222 infiltrating lymphocytes (TIL), pairwise comparisons between  
223 treatment groups were performed by unpaired *t* tests. All hypoth-  
224 esis testing was two-sided, and a significance threshold of 0.05 for  
225 *P* value was used.

## 226 Results

### 227 *In vivo* syngeneic animal models with differential responses to 228 PD-1 pathway blockade

229 In order to have animal models that consistently respond to  
230 anti-PD-1 therapy, we tested four melanoma models, three  
231 derived from *BRAF*<sup>V600E</sup>/*PTEN*<sup>-/-</sup> genetically engineered mice  
232 (Supplementary Fig. S1A) and B16, and compared them with  
233 MC38, a cell line that has been previously shown to respond well  
234 to PD-1 blockade therapy (30, 31). In three replicate studies, we  
235 observed antitumor activity of anti-PD-1 or anti-PD-L1 antibody  
236 therapy against MC38 (Fig. 1A) and YUMM2.1 (Fig. 1B), but no  
237 antitumor activity against YUMM1.1 (Fig. 1C), YUMM1.7, or B16  
238 (Supplementary Fig. S1B). Of note, these responses to anti-PD-1  
239 antibody are incomplete, and both MC38 and YUMM2.1 tumors  
240 start regrowing around days 35 to 40 after tumor injection. We  
241 decided to focus our further mechanistic studies in MC38 for a  
242 tumor that is known to respond to anti-PD-1, and studied the  
243 differential responses in YUMM1.1 and YUMM2.1.

### 244 Similar PD-L1 expression induced in MC38, YUMM2.1, and 245 YUMM1.1 by IFN $\gamma$

246 In order to investigate the mechanism of response to anti-PD-1  
247 therapy, we first focused on induced PD-L1 expression in these  
248 three cell lines. Total cellular PD-L1 increased upon exposure to  
249 IFN $\gamma$  in the three cell lines, with a higher magnitude of increase in  
250 MC38 cells than in YUMM2.1 and YUMM1.1 cells (Fig. 2A).

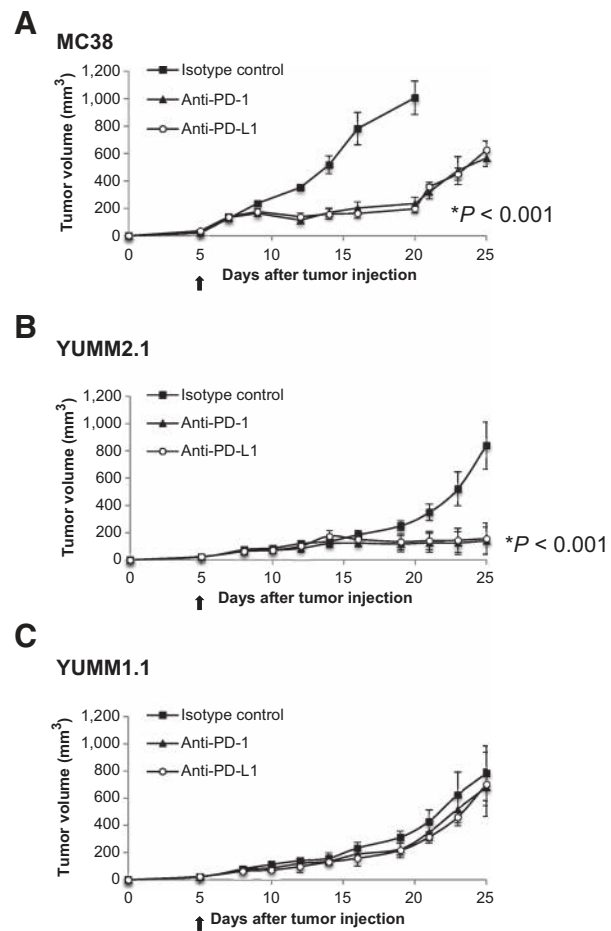


**Figure 1.**

Enhanced *in vivo* antitumor activity with anti-PD-1 or anti-PD-L1 in MC38 and YUMM2.1 tumor models compared with YUMM1.1. Tumor growth curves of MC38 (A), YUMM2.1 (B), and YUMM1.1 C, with 4 mice in each group (mean  $\pm$  SD) after anti-PD-1, anti-PD-L1, or isotype control. The arrow indicates the day when treatment with anti-PD-1, anti-PD-L1, or isotype control was started. \*, *P* < 0.001 by unpaired *t* test on day 20, anti-PD-1 versus isotype control, anti-PD-L1 versus isotype control in MC38, anti-PD-1 versus isotype control, anti-PD-L1 versus isotype control in YUMM2.1 tumors.

Q10

Surface expression of PD-L1 was low at baseline, and increased upon exposure to IFN $\gamma$  in the three cell lines, though less evident in the morphologically more heterogeneous YUMM1.1 cell line (Fig. 2B).

### 256 Increased mutational load in MC38 compared with YUMM1.1 257 and YUMM2.1

258 Next, we determined whether mutational load is a contributor  
259 to the observed differential response to anti-PD-1 therapy. MC38,  
260 which was established from a mouse exposed to the carcinogen  
261 dimethylhydralazine (32), has a higher mutational load (2,778  
262 mutations), compared with the much lower mutational rates in  
263 YUMM1.1 and YUMM2.1 (128 and 68 nonsynonymous variants,  
264 respectively; Supplementary Fig. S1C). Despite independent der-  
265 ivation, 26 variants are shared by YUMM1.1 and YUMM2.1,  
266 which likely represent SNPs not found in the sequenced strain-  
267 matched control or in the National Center for Biotechnology

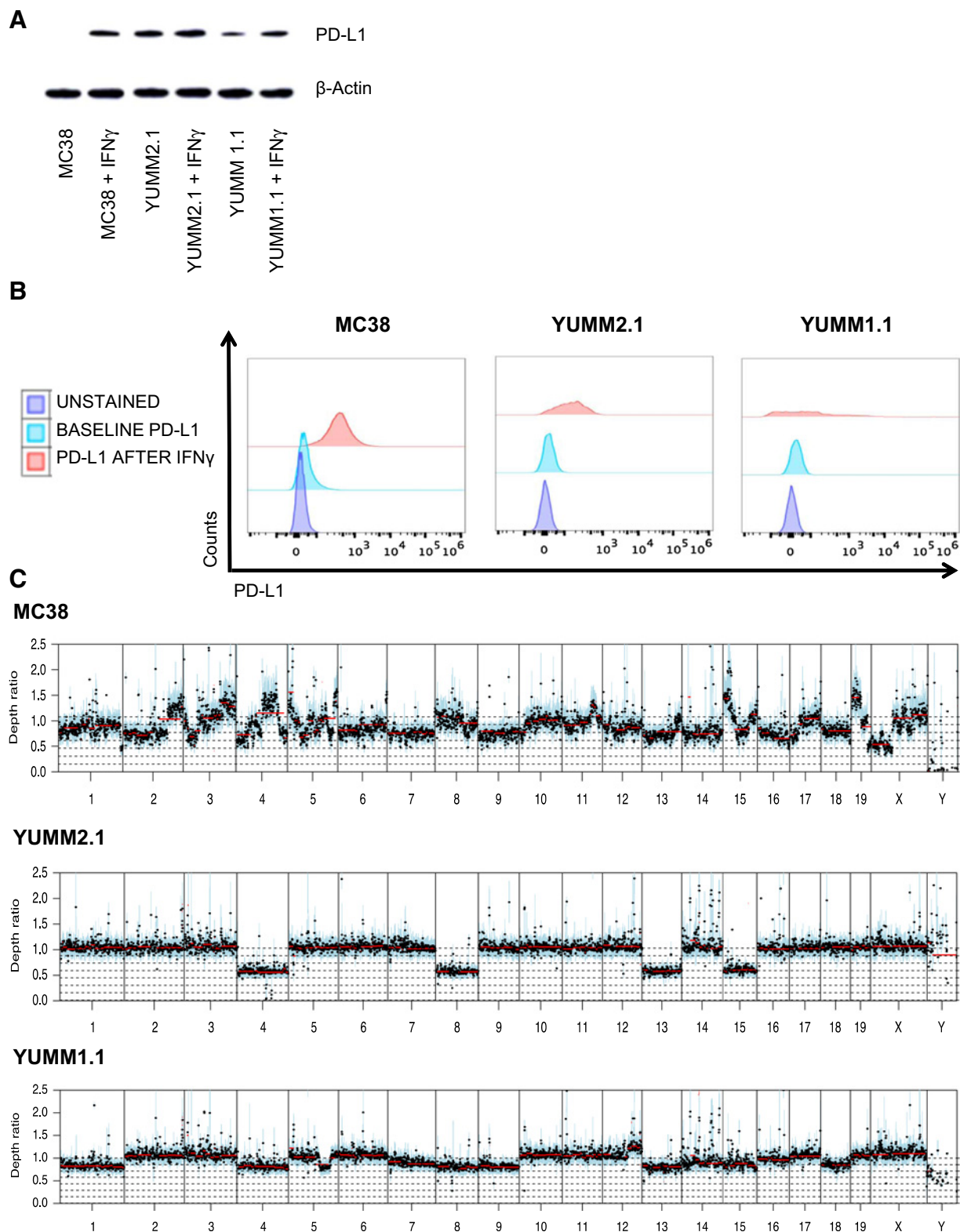


**Figure 2.** IFN $\gamma$  modulates PD-L1 expression in MC38, YUMM2.1, and YUMM1.1. **A**, Western blot analysis of PD-L1. MC38, YUMM2.1, and YUMM1.1 cells were cultured with or without IFN $\gamma$  for 24 hours. **B**, expression of PD-L1 by flow cytometry on MC38, YUMM2.1, and YUMM1.1 cells at baseline and after 24 hours of stimulation with IFN $\gamma$ . **C**, chromosomal copy-number variation in MC38, YUMM2.1, and YUMM1.1 cell lines. Y-axis represents Log<sub>2</sub> depth ratio vs. matched normal.

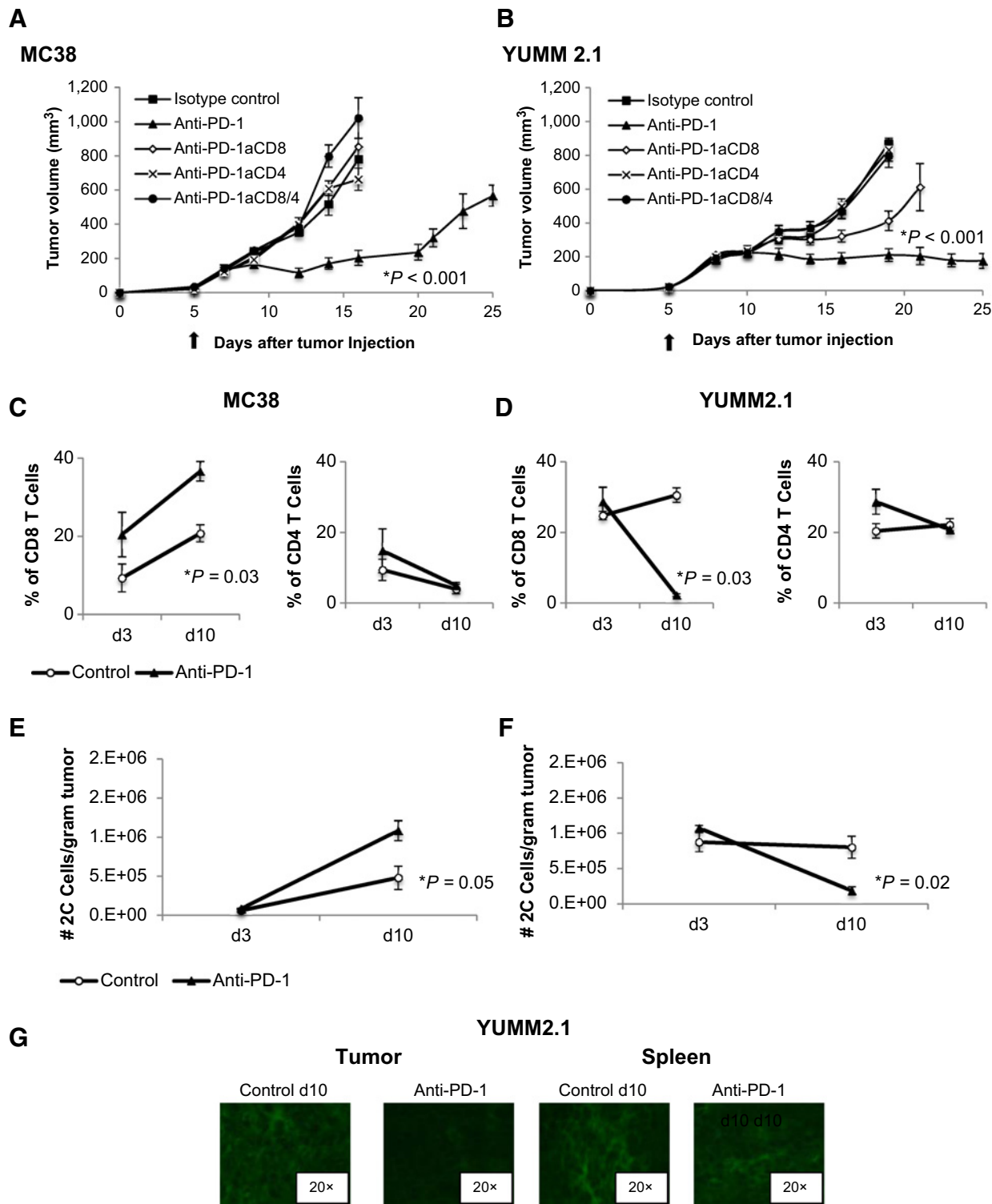


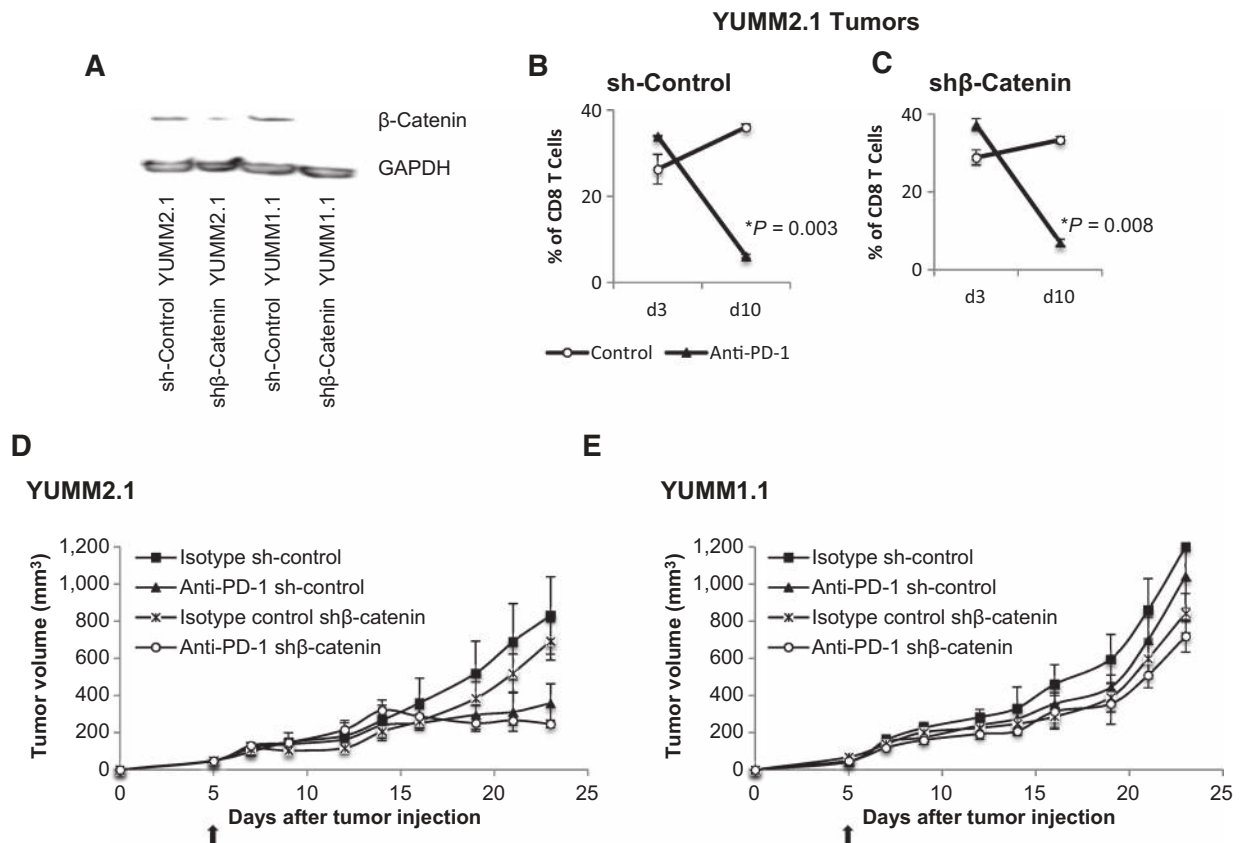
**Figure 3.** Both CD8 and CD4 cells mediate response to PD-1 blockade in MC38 and YUMM2.1. Tumor growth curves of MC38 (A) and YUMM2.1 (B) after anti-PD-1 and either anti-CD8 (anti-PD-1aCD8), anti-CD4 (anti-PD-1aCD4), anti-CD8 + anti-CD4 (anti-PD-1aCD8/4) or isotype control; 4 mice in each group, mean  $\pm$  SD. (\*,  $P < 0.001$  isotype control, anti-PD-1aCD8, anti-PD-1aCD4, anti-PD-1aCD8/4 versus anti-PD-1 in MC38,  $P < 0.001$  isotype control, anti-PD-1aCD4, anti-PD-1aCD8/4 versus anti-PD-1 in YUMM2.1, unpaired  $t$  test,  $n = 4$ ); \*,  $P = 0.003$  anti-PD-1aCD8 versus anti-PD-1, unpaired  $t$  test,  $n = 4$ . The arrow indicates the day treatment with anti-PD-1 or isotype control was started. This experiment was performed in triplicate. (Continued on the following page)



270	Information database of genetic variation. Copy-number varia-	<b>Wnt/<math>\beta</math>-catenin uninvolved in YUMM2.1 CD8 T-cell decrease or</b>	322
271	tion analysis revealed substantial differences in chromosomal	<b>response to anti-PD-1</b>	323
272	alteration patterns between the three cell lines (Fig. 2C). However,	YUMM2.1 cell line was derived from a mouse with the same	324
273	most are shallow amplifications or deletions ( $\log_2$ ratio between	genetic background as YUMM1.1 but containing an additional	325
274	0.5 and 1.5).	transgenic allele that, when recombined by tamoxifen induction,	326
275		produces a stabilized $\beta$ -catenin, which leads to increased meta-	327
276	<b>CD8 and CD4 T cells important in response to PD-1 blockade in</b>	static potential of the tumors (33). However, whole-exome	328
277	<b>MC38 and YUMM2.1</b>	sequencing and PCR showed that $\beta$ -catenin was unrecombined	329
278	To elucidate the role of CD8 and CD4 T cells in anti-PD-1	in the YUMM2.1 cell line, and the recombination could be	330
279	activity, both cell subtypes were depleted in C57BL/6 mice bear-	induced by tamoxifen (4HT; Supplementary Fig. S3A and S3B).	331
280	ing MC38 or YUMM2.1 tumors. Antibody-mediated depletion	Nevertheless, we observed that YUMM2.1 cells do have more	332
281	was confirmed in YUMM2.1 tumors and spleens (Supplementary	$\beta$ -catenin protein expression with increased activity tested <i>in vitro</i>	333
282	Fig. S2A and S2B). In the absence of CD8 cells, CD4 cells, or both,	(Supplementary Fig. S3C) and in macro-dissected tumor sections	334
283	antitumor response diminished in both MC38 and YUMM2.1	when implanted in mice (Supplementary Fig. S3D). Active Wnt/ $\beta$ -	335
284	models (Fig. 3A and B). Of note, CD8 cell depletion (anti-PD-	catenin was linked to T-cell exclusion in tumors (34). To test if	336
285	1aCD8) in the YUMM2.1 tumor model only partially abrogated	$\beta$ -catenin had a role in the immunogenicity of YUMM2.1 and the	337
286	the response to anti-PD-1 therapy, whereas CD4 cell depletion, or	loss of CD8 infiltrates on day 10 after anti-PD-1 therapy, $\beta$ -cate-	338
287	CD4 plus CD8 depletion, completely abrogated this response	nin in both YUMM2.1 and YUMM1.1 cell lines was knocked	339
	(Fig. 3B).	down and confirmed at the protein level (Fig. 4A). Knockdown of	340
		$\beta$ -catenin in YUMM2.1 did not change the significant decrease of	341
		CD8 T cells on day 10 with anti-PD-1 treatment when compared	342
288	<b>Increased TILs in MC38, but decreased in YUMM2.1, upon PD-1</b>	with the respective isotype-treated controls (Fig. 4B and C).	343
289	<b>blockade</b>	Silencing $\beta$ -catenin did not change the antitumor response in the	344
290	Three and ten days after starting treatment with anti-PD-1 or	YUMM2.1 model (Fig. 4D), nor did it change in the nonrespon-	345
291	isotype control, tumors and spleens were harvested and stained	sive YUMM1.1 model (Fig. 4E).	346
292	for CD3, CD4, and CD8 (Supplementary Fig. S2C and S2D). CD8		
293	T-cell infiltration increased in MC38 tumors (calculated as per-	<b>Requirement of costimulation with PD-1 blockade in YUMM2.1</b>	347
294	centage of all cells in the tumor) on day 3 and day 10 of treatment	The evidence that both CD4 and CD8 cells are required for	348
295	with anti-PD-1 when compared with isotype control (Fig. 3C),	response to PD-1 blockade in the MC38 and YUMM2.1 models	349
296	whereas CD8 T cells in the corresponding spleens of MC38	suggests that T-cell priming and CD4 helper function may be	350
297	tumor-bearing mice remained unchanged (Supplementary Fig.	needed to induce the cytotoxic response to the tumors, which was	351
298	S2E). No significant difference in the percentage of CD4 T cells was	further studied. The antitumor activity of PD-1 blockade against	352
299	observed in MC38 tumors (Fig. 3C) and spleens (Supplementary	YUMM2.1 was completely abolished in CD28 knockout (KO; Fig.	353
300	Fig. S2F). However, CD8 T-cell infiltration into YUMM2.1 tumors	5A) and CD80/CD86 double KO mice (Fig. 5B), clearly demon-	354
301	was significantly decreased on day 10 of anti-PD-1 therapy when	strating that costimulation is a requirement for the efficacy of	355
302	compared with isotype control. This decrease in CD8 T cells was	anti-PD-1 blockade in this model.	356
303	not present on day 3 (anti-PD-1 d3) compared with isotype		
304	control group (Fig. 3D). CD8 T cells did not decrease in the	<b>Increased antigen-presenting dendritic cells in anti-PD-1-</b>	357
305	corresponding spleens of any of the conditions in the YUMM2.1	<b>treated YUMM2.1 tumors</b>	358
306	model (Supplementary Fig. S2E). The percentage of CD4 T cells in	The next step was to identify the cells involved in antigen	359
307	the YUMM2.1 tumors or spleens was not significantly different	presentation and costimulation. We phenotyped the different	360
308	across different time points or between anti-PD-1 and isotype	subtypes of dendritic cells (DC) by staining for CD11c <sup>+</sup> B220 <sup>-</sup>	361
309	control tumors (Fig. 3D). The YUMM1.1 tumor model did not	(conventional) and CD11c <sup>+</sup> B220 <sup>+</sup> (plasmacytoid) subsets. Con-	362
310	show any CD8 T-cell variation in either tumors or spleens com-	ventional DCs can be further subdivided into CD11c <sup>+</sup>	363
311	paring anti-PD-1 and isotype control-treated conditions (Sup-	B220 <sup>-</sup> CD8 <sup>+</sup> DCs, which are CD103 <sup>+</sup> in peripheral tissues and	364
312	plementary Fig. S2G). When we calculated the absolute number of	have been reported to mediate antigen cross-presentation to CD8	365
313	CD8 T cells per gram of tumor pooled from two separate experi-	T cells (35), and CD11c <sup>+</sup> CD11b <sup>+</sup> MHC-II <sup>high</sup> DCs, which are	366
314	ments, it confirmed the significant increase in CD8 T cells in the	considered to be dedicated APCs that present peptides on	367
315	MC38 tumors (Fig. 3E) and the significant decrease in CD8 T cells	MHC-II molecules to CD4 T cells (ref. 36; gating strategy in	368
316	in the YUMM2.1 tumors on day 10 of anti-PD-1 treatment (Fig.	Supplementary Fig. S4A and S4B). The percentage of CD11c <sup>+</sup>	369
317	3F). Immunofluorescence staining of tumors and spleens from	B220 <sup>-</sup> cells was significantly decreased in MC38 tumors of mice	370
318	mice in the YUMM2.1 group collected after anti-PD-1 therapy or	treated with anti-PD-1 compared with isotype control, with no	371
319	isotype control also demonstrated a remarkable decrease in intra-	significant change in YUMM2.1 or YUMM1.1 tumors (Fig. 5C).	372
320	tumoral CD8 T cells on day 10 and no change in spleen (Fig. 3G).		

(Continued.) On days 3 (d3) and 10 (d10) after treatment with anti-PD-1 or isotype control was started, MC38 and YUMM2.1 tumors were isolated and stained with fluorescent-labeled antibodies, analyzed by FACS. **C** and **D**, percentage of CD3<sup>+</sup>CD8<sup>+</sup> (CD8 T cells) and CD3<sup>+</sup>CD4<sup>+</sup> (CD4 T cells) in MC38 (**C**) and YUMM2.1 (**D**), tumors are shown (mean  $\pm$  SD). \*,  $P = 0.03$  anti-PD-1 d10 versus control d10 in MC38;  $P = 0.03$  anti-PD-1 d10 versus control d10 in YUMM2.1 (unpaired  $t$  test,  $n = 4$ ). Results were consistent in 6 replicate experiments. **E** and **F**, statistical analysis of the 2C total number of CD8 T cells per gram of tumor in MC38 (**E**) and (**F**) YUMM2.1 tumors. \*,  $P = 0.05$  anti-PD-1 d10 versus control d10 in MC38,  $P = 0.02$  anti-PD-1 d10 versus control d10 in YUMM2.1, unpaired  $t$  test,  $n = 8$ . **G**, representative immunofluorescence of CD8 T cells stained in YUMM2.1 tumors and spleens d10 after treatment with anti-PD-1 or isotype control was started.

Q11

**Figure 4.**

Wnt/ $\beta$ -catenin pathway is not involved in CD8 T-cell decrease or anti-PD-1 antitumor response in YUMM2.1 tumor model. **A**, Western blot analysis of  $\beta$ -catenin in YUMM2.1 cells transduced with shRNA without  $\beta$ -catenin (sh YUMM2.1) or with sh $\beta$ -catenin (sh $\beta$ -catenin YUMM2.1) and YUMM1.1 cells transduced with shRNA without  $\beta$ -catenin (sh YUMM1.1) or with sh $\beta$ -catenin (sh $\beta$ -catenin YUMM1.1). **B**, quantification of CD3<sup>+</sup>CD8<sup>+</sup> (CD8 T cells). Tumor cells harvested on days 3 and 10 after anti-PD-1 or isotype control were counted and analyzed by flow cytometry for CD3/CD8 staining; 3 mice in each group (mean  $\pm$  SD). \*,  $P = 0.003$  anti-PD-1 d10 versus control d10 in sh-control YUMM2.1 tumors. **C**, sh $\beta$ -catenin YUMM2.1 tumors. \*,  $P = 0.008$  anti-PD-1 d10 versus control d10 in sh $\beta$ -catenin YUMM2.1 tumors, unpaired  $t$  test,  $n = 4$ . **(D)** *in vivo* sh and sh $\beta$ -catenin YUMM2.1 and **(E)** sh and sh $\beta$ -catenin YUMM1.1 tumor growth curves with 3 to 4 mice in each group (mean  $\pm$  SD) after anti-PD-1 or isotype control.

375 The percentage of intratumoral CD11c<sup>+</sup>B220<sup>-</sup>CD8<sup>+</sup> and CD11c<sup>+</sup>  
 376 B220<sup>-</sup>CD103<sup>+</sup> DCs in MC38, YUMM2.1, or YUMM1.1 was not  
 377 significantly different across time points or with PD-1 blockade  
 378 therapy. A very small percentage of CD11c<sup>+</sup>B220<sup>-</sup>CD8<sup>+</sup> cells in  
 379 YUMM2.1 tumors were present (Fig. 5D). Growth of tumors in  
 380 mice that were CD103-depleted was analogous to nondepleted  
 381 mice, with or without the addition of anti-PD-1 (Fig. 5E). Of note,  
 382 anti-PD-1-treated YUMM2.1 tumors exhibited a significant  
 383 increase in CD11c<sup>+</sup>CD11b<sup>+</sup> and CD11c<sup>+</sup>CD11b<sup>+</sup>MHC-II<sup>high</sup>  
 384 DCs compared with isotype control-treated tumors (Fig. 5F).  
 385 This finding was not present in MC38 tumors.

#### 386 Increased tumor-associated macrophages in YUMM2.1 tumors 387 treated with anti-PD-1

388 Another immune cell subtype potentially implicated in T-cell  
 389 priming are tumor-associated macrophages (TAM). CD11b<sup>+</sup>F4/  
 390 80<sup>+</sup> TAMs were gated after the exclusion of dead cells (Supple-  
 391 mentary Fig. S4C). The total percentage of TAMs decreased (not  
 392 statistically significant) in MC38 tumors treated with anti-PD-1  
 393 (Fig. 6A). In contrast, TAMs significantly increased in YUMM2.1  
 394 tumors on day 10 after anti-PD-1 treatment was started. Immune-

suppressive TAMs (CD11b<sup>+</sup>F4/80<sup>+</sup>MHC-II<sup>low</sup>, M2 TAMs) were  
 more frequent in YUMM2.1 tumors with or without anti-PD-1  
 therapy, with an increase in the percentage of both CD11b<sup>+</sup>F4/  
 80<sup>+</sup>MHC-II<sup>high</sup> TAMs (M1 TAMs) and M2 TAMs upon PD-1  
 blockade (Fig. 6B). These observations were not present in  
 YUMM1.1 tumors, where TAMs remained mostly unchanged (Fig.  
 6B). Taken together, TAMs may play a different role in YUMM2.1  
 tumors compared with MC38, although both tumor models  
 respond to anti-PD-1 blockade.

#### No change in MDSCs or regulatory T cells with PD-1 blockade therapy

To evaluate the effect of anti-PD-1 on other cellular compo-  
 nents of the tumor microenvironment, we harvested tumors 10  
 days after anti-PD-1 treatment was started and analyzed the two  
 main subsets of myeloid-derived suppressor cells (MDSC):  
 monocytic MDSCs (MO-MDSC, CD11b<sup>+</sup>Ly6C<sup>high</sup>Ly6G<sup>low</sup>) and  
 polymorphonuclear MDSCs (PMN-MDSC, CD11b<sup>+</sup>Ly6C<sup>low</sup>Ly6-  
 G<sup>high</sup>; Supplementary Fig. S4D). Anti-PD-1 did not change  
 the percentage of MO-MDSCs or PMN-MDSC in any  
 tumors compared with isotype control (Fig. 6C). Another



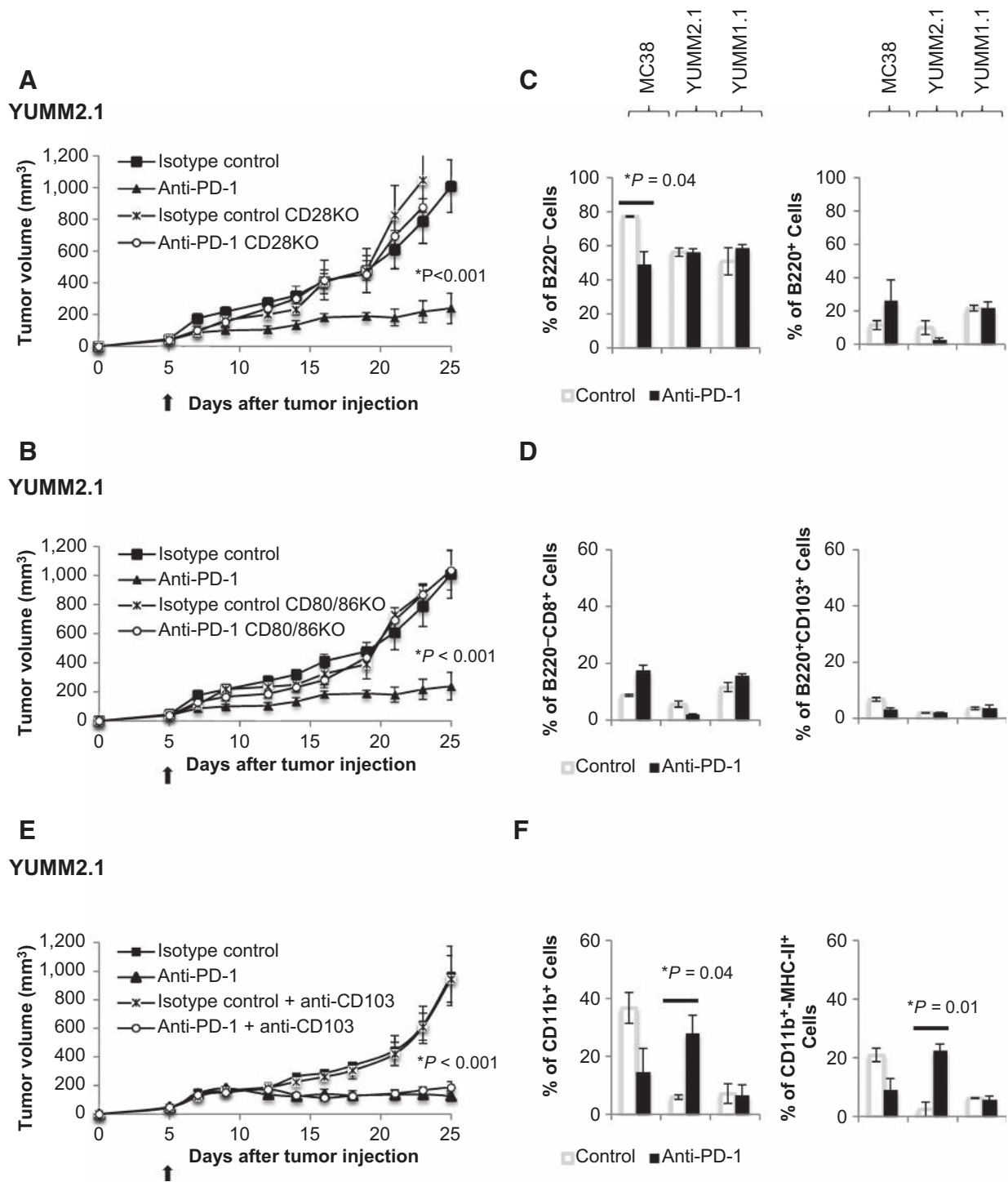


**Figure 5.** Increased antigen-presenting DCs in anti-PD-1-treated YUMM2.1 tumors. **A**, tumor growth curves of CD28KO or C57BL/6 mice bearing YUMM2.1 treated with anti-PD-1 or isotype control. **B**, tumor growth curves of CD80/86KO or C57BL/6 mice bearing YUMM2.1 treated with anti-PD-1 or isotype control. Four mice in each group (mean ± SD). The arrow indicates the day treatment with anti-PD-1 or isotype control was initiated. **C**, on day 10 after starting treatment, MC38, YUMM2.1, and YUMM1.1 tumors were isolated and stained with fluorescent-labeled antibodies and analyzed by FACS, with 3 mice in each group (mean ± SD). B220<sup>-</sup> and B220<sup>+</sup> cells presented as percentage of CD11c<sup>+</sup> cells. \*, *P* = 0.04 anti-PD-1 versus isotype control, CD11c<sup>+</sup>B220<sup>-</sup> cells in MC38 tumors, unpaired *t* test, *n* = 3. **D**, B220<sup>-</sup>CD8<sup>+</sup> and B220<sup>+</sup>CD103<sup>+</sup> presented as percentage of CD11c<sup>+</sup> cells. **E**, *in vivo* YUMM2.1 growth curve after anti-PD-1 ± anti-CD103 or isotype control ± anti-CD103, 4 mice in each group (mean ± SD). The arrow indicates the day anti-PD-1 or isotype control treatment was started. **F**, CD11b<sup>+</sup> and CD11b<sup>+</sup>MHC-II<sup>high</sup> DCs presented as percentage of CD11c<sup>+</sup> cells. \*, *P* = 0.04 anti-PD-1 versus control, *P* = 0.01 anti-PD-1 versus control in YUMM2.1 tumors, unpaired *t* test, *n* = 3.

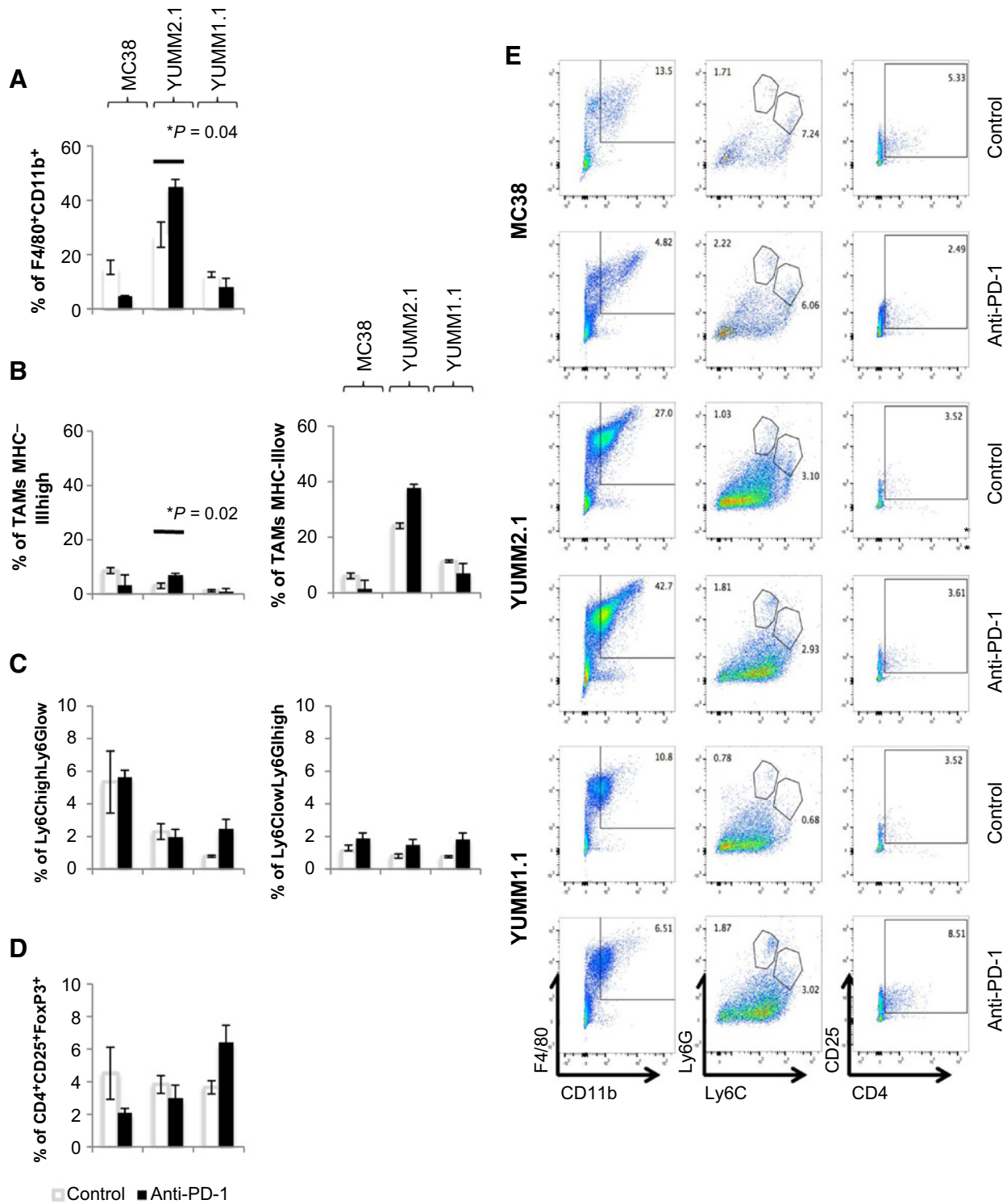


**Figure 6.** Modulation of the tumor microenvironment by anti-PD-1 in MC38, YUMM2.1, and YUMM1.1. On day 10 after anti-PD-1 or isotype control, MC38, YUMM2.1, and YUMM1.1 tumors were isolated and stained with fluorescent-labeled antibodies and analyzed by FACS, with 3 mice in each group (mean  $\pm$  SD). **A**, analysis of TAMs (CD11b<sup>+</sup>F4/80<sup>+</sup>). **B**, TAMs MHC-II<sup>high</sup> (M1 TAMs, CD11b<sup>+</sup>F4/80<sup>+</sup>MHC-II<sup>high</sup>) and TAMs MHC-II<sup>low</sup> (M2 TAMs, CD11b<sup>+</sup>F4/80<sup>+</sup>MHC-II<sup>low</sup>). \*,  $P = 0.04$  anti-PD-1 d10 versus control d10 TAMs;  $P = 0.02$  anti-PD-1 d10 versus control d10 TAMs MHC-II<sup>high</sup> in YUMM2.1 tumors, unpaired  $t$  test,  $n = 3$ . **C**, MO-MDSC (CD11b<sup>+</sup>Ly6C<sup>high</sup>Ly6G<sup>low</sup>) and PMN-MDSC (CD11b<sup>+</sup>Ly6C<sup>low</sup>Ly6G<sup>high</sup>) presented as percentage of CD11b<sup>+</sup> cells. **D**, analysis of T<sub>regs</sub> (CD4<sup>+</sup>CD25<sup>+</sup>FOXp3<sup>+</sup>). **E**, representative FACS plots in tumors.

418 immune-suppressive cell population, regulatory T cells ( $T_{reg}$ ;  
 419 Supplementary Fig. S4E;  $T_{reg}$ ,  $CD4^+CD25^+FOXP3^+$ ), showed a  
 420 nonstatistically significant trends toward a decrease in MC38 and  
 421 YUMM2.1 tumors with anti-PD-1 and an increase in YUMM1.1  
 422 (Fig. 6D). Representative flow charts of TAMs, MDSCs, and  $T_{reg}$   
 423 are shown in Fig. 6E.

424 **A more inflammatory gene signature profile in YUMM2.1**  
 425 **compared with YUMM 1.1**

426 RNA was extracted from cultured YUMM1.1 and YUMM2.1 and  
 427 subjected to RNA sequencing. GSEA and pathway analyses indicated  
 428 that immune response, cytokine production, and inflam-  
 429 matory-related genes were strongly represented in YUMM2.1  
 430 compared with YUMM = 1.1 cells (Fig. 7A). Corresponding  
 431 normalized enrichment scores (NES), *P* values, and FDR of the  
 432 GSEA plots are included (Fig. 7B). Analysis of genes that code for  
 433 secreted proteins with a  $\log_2$ -fold higher than 1 in YUMM2.1  
 434 compared with YUMM1.1 cells revealed an increase in inflam-  
 435 matory and chemotaxis-related genes (Supplementary Fig. S4F).

436 **Discussion**

437 Immunological checkpoint blockade with anti-PD-1 or anti-  
 438 PD-L1 antibodies reverses cancer immunosuppression and

440 promotes antitumor immune responses in several cancer types.  
 441 Long-term responses with minimal side effects have been reported  
 442 in patients with melanoma, lung, liver, kidney, bladder, mismatch  
 443 repair-deficient colon cancers, and hematologic malignancies,  
 444 among others (1–4, 31). Why these agents exhibit antitumor  
 445 responses in certain histologies and only in a percentage of  
 446 patients with the same type of tumor remains unknown. Here,  
 447 we studied tumor models that respond differently to anti-PD-1  
 448 treatment and tested the reasons for anti-PD-1 activity in MC38  
 449 and YUMM2.1 tumors.

450 Upregulation of PD-L1 and its ligation to PD-1 on activated T  
 451 cells is a well-described mechanism by which cancer tissues limit  
 452 the host immune response, termed adaptive immune resistance  
 453 (37). High baseline PD-L1-expressing tumor cells have been  
 454 positively correlated with response to PD-1 blockade in patient  
 455 samples (5, 6). However, PD-L1 was markedly increased  
 456 upon  $IFN\gamma$  exposure in the three murine cell lines studied, which  
 457 does not provide an explanation for the different responses to  
 458 anti-PD-1.

459 Mutational load has been associated with a higher clinical  
 460 benefit to immunotherapy (38–40). A greatly increased number  
 461 of somatic mutations were observed in MC38 compared with  
 462 YUMM2.1 and YUMM1.1, accompanied by high copy-number  
 463 variation, consistent with its origin as a carcinogen-induced cell

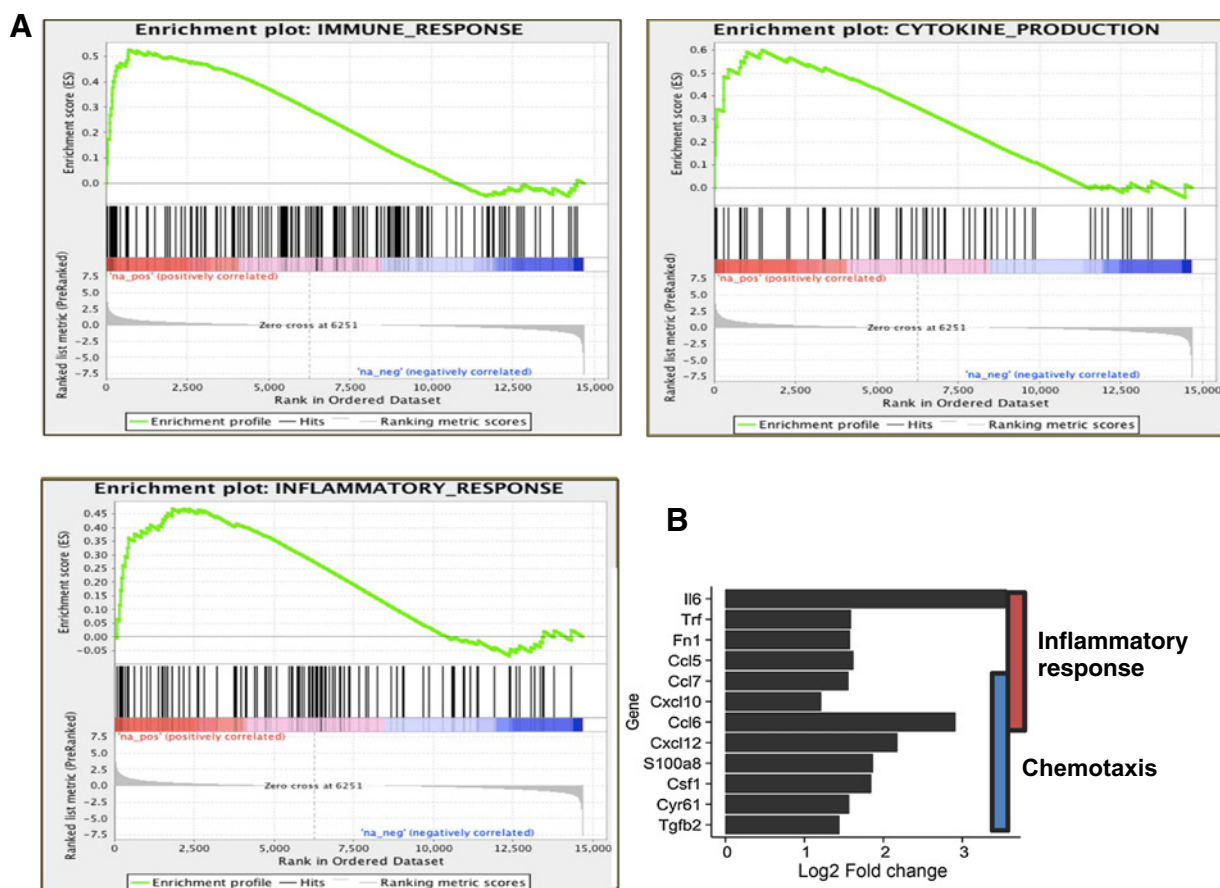


**Figure 7.** YUMM2.1 is more inherently immune permissive than YUMM1.1. **A**, GSEA curves for YUMM2.1 versus YUMM1.1 enriched pathways involved in immune response, cytokine production, and inflammatory response. **B**, corresponding NES, *P* values, and FDR of the GSEA plots.

466	line. The high mutational load could be at least partially respon-	528
467	sible for the effectiveness of anti-PD-1 therapy in MC38 tumors.	529
468	However, both YUMM2.1 and YUMM1.1 displayed a very low	530
469	number of new somatic mutations, consistent with tumors arising	531
470	from genetically engineered mice driven by a strong driver onco-	532
471	gene and avoidance of senescence.	533
472	T-cell response has been widely accepted to be crucial for	534
473	effective anti-PD-1/PD-L1 antitumor activity (41). We confirmed	535
474	the essential roles of both the CD8 and CD4 T cells in anti-PD-1	536
475	effect in both MC38 and YUMM2.1 tumor models. Depletion of	537
476	CD8 cells completely abrogated the antitumor effect of PD-1	538
477	blockade in the MC38 model but only had a partial effect in the	539
478	YUMM2.1 model, whereas CD4 depletion completely reversed	540
479	the antitumor effect in both models. Considering that anti-PD-1	541
480	also controls key T-cell inhibitory interactions between PD-L1 on	542
481	APCs and PD-1 on T cells (17, 42) and that PD-1 limits CD4 T-cell	543
482	clonal expansion in response to an immunogenic stimulus (43), it	544
483	is not surprising that CD4 T cells are required for anti-PD-1/PD-	545
484	L1 tumor response. However, another group has reported oppo-	546
485	site observations, with increased antitumor effect seen with CD4	547
486	cell depletion combined with PD-1/PD-L1 blockade (44). Of	548
487	note, none of the tumor models evaluated by this group was	549
488	responsive to anti-PD-1/PD-L1 itself. The authors suggested that	550
489	CD4 cell depletion effect was partially attributed to a removal of	551
490	CD4-positive immunosuppressive T <sub>regs</sub> . However, in another	552
491	report (31), T <sub>regs</sub> increased after very early analysis (48 and 72	553
492	hours) following treatment with anti-PD-1 in MC38, whereas in	554
493	our tumor models, T <sub>regs</sub> did not change with anti-PD-1 when	555
494	analyzed at 10 days after starting therapy.	556
495	Next, we characterized anti-PD-1 modulation of the cellular	557
496	components in the tumor microenvironment. CD8 T cells were	558
497	expected to increase in both anti-PD-1-responsive tumors. This	559
498	was true for MC38, but in YUMM2.1, CD8 T cells decreased over	560
499	time with anti-PD-1 therapy, implying that CD8 T cells may have	561
500	an early role in this antitumor response. Therefore, the early	562
501	activation of CD8 T cells could take place during antigen presen-	563
502	tation to naïve T cells, where PD-1/PD-L1 costimulation has been	564
503	shown to lead to T-cell receptor (TCR) downmodulation (16, 17,	565
504	42). DCs have been reported to hyperactivate CD8 T cells in the	566
505	absence of PD-1/PD-L1 costimulation, which was accompanied	567
506	by a higher TCR surface level and an increase in IFN $\gamma$ (17).	568
507	Depending on where PD-1/PD-L1 blockade takes place, T-cell	569
508	activity may vary. It is unknown if the location of PD-1/PD-L1	570
509	interaction and its consecutive blockade is tumor-dependent in a	571
510	short-term implanted tumor model. Functional studies to deter-	572
511	mine T-cell activity shortly after anti-PD-1 are administered, and	573
512	further characterization of the specific CD8 T-cell phenotype	
513	could provide some explanation on how CD8 T cells exhibit their	
514	effect in this tumor model. The role of natural killer (NK) cells in	
515	this setting is unknown and technically challenging because of	
516	their low frequency in the tumor microenvironment, but certainly	
517	interesting to explore. Differences in PD-1 expression on the CD8	
518	T cells could also be informative to address PD-1 responsiveness	
519	in the YUMM2.1 tumor model, as shown by others (31).	
520	The correlation between tumor-intrinsic stabilized $\beta$ -catenin	
521	and both T-cell exclusion and anti-PD-L1 resistance in genetically	
522	engineered mice with <i>BRAF</i> <sup>V600E</sup> / <i>PTEN</i> <sup>-/-</sup> / <i>\beta</i> -catenin-stabilized	
523	tumors (34) led us to investigate the effect of $\beta$ -catenin down-	
524	regulation in T-cell modulation and anti-PD-1 antitumor	
525	response. Although our analysis indicated that YUMM2.1 did	
526	not have recombined $\beta$ -catenin allele that would render $\beta$ -catenin	
	more stable, it does have more $\beta$ -catenin expression and activity	
	compared with the other YUMM cell lines. We observed that T	
	cells were reduced over time (but never upfront excluded) with	
	anti-PD-1 therapy, and this phenomenon was independent from	
	the $\beta$ -catenin status. PD-1 blockade antitumor effect was not	
	altered in the presence of a downregulated Wnt/ $\beta$ -catenin	
	pathway.	
	Looking further into the importance of costimulatory	
	interactions during antigen presentation to naïve T cells, we	
	demonstrated that the absence of CD28 or CD80/86 prevented	
	the anti-PD-1 effects in YUMM2.1 tumors. This observation does	
	not necessarily imply that the PD-1/PD-L1 inhibitory effects only	
	take place at the APC-T-cell synapse, but suggest that PD-L1-	
	expressing APCs are positively enhanced upon PD-1 blockade.	
	Indeed, the priming of CD4 and CD8 T cells is more effective in	
	the absence of PD-1/PD-L1 signaling (45), and downmodulation	
	of PD-L1 in DCs results in increased costimulatory molecule	
	CD80 expression and a distinct cytokine profile (46). The same	
	group observed strong tumor growth control when using PD-L1-	
	silenced DCs in a mouse model of lymphoma, although with no	
	increased cure rates, possibly due to PD-L1-expressing tumor cells	
	that might counteract CD8 T-cell activity (47).	
	Analysis of the different DC subsets in YUMM2.1 tumors	
	revealed an increase in CD11c <sup>+</sup> CD11b <sup>+</sup> MHC-II <sup>high</sup> DCs upon	
	PD-1 blockade, which was not present in the other tumor models	
	analyzed. Cross-priming of tumor antigens by BATF3-dependent	
	DCs is crucial to the efficacy of anti-PD-1 antibodies (48). Taken	
	together, these data imply that priming via CD4 T cells has a more	
	important role in the antitumor efficacy of PD-1 blockade in the	
	YUMM2.1 model.	
	When looking into the ability of the models to evoke an	
	inflammatory reaction required for immune cell recruitment and	
	DC-T-cell costimulation, YUMM2.1 exhibited an "inflammatory	
	profile" consistent with an endogenous upregulation of immune,	
	cytokine producing, and inflammatory response-related genes.	
	The YUMM2.1 model could therefore intrinsically harbor inflam-	
	matory mediators necessary to couple innate recognition to	
	T-cell-mediated immunity by DCs <i>in vivo</i> , which is also supported	
	by the increase in chemotactic factors such as Cxcl10, Ccl6, or	
	Cxcl12. This observation is consistent with other reports, where	
	chemokine-trafficking of immune cells into tumors was observed	
	in human melanoma cell lines (49) or in mice receiving adoptive	
	cell therapy and anti-PD-1 blockade (50).	
	In conclusion, T-cell priming supports anti-PD-1 antitumor	
	responses mediated by CD4 and CD8 T cells, critically requiring	
	costimulation <i>in vivo</i> .	
	<b>Disclosure of Potential Conflicts of Interest</b>	574
	No potential conflicts of interest were disclosed.	Q13575
	<b>Authors' Contributions</b>	576
	<b>Conception and design:</b> B. Homet Moreno, A. Garcia-Diaz, S. Hu-Lieskovan,	577
	A. Ribas	578
	<b>Development of methodology:</b> B. Homet Moreno, A. Garcia-Diaz, M. Bosen-	579
	berg, B. Comin-Anduix, S. Hu-Lieskovan, A. Ribas	580
	<b>Acquisition of data (provided animals, acquired and managed patients,</b>	581
	<b>provided facilities, etc.):</b> B. Homet Moreno, L. Robert, K. Meeth, A.T. Weerar-	582
	atna, S. Hu-Lieskovan, A. Ribas	583
	<b>Analysis and interpretation of data (e.g., statistical analysis, biostatistics,</b>	584
	<b>computational analysis):</b> B. Homet Moreno, J.M. Zaretsky, J. Tsoi, M. Bosen-	585
	berg, A.T. Weeraratna, T.G. Graeber, B. Comin-Anduix, S. Hu-Lieskovan,	586
	A. Ribas	587

590 **Writing, review, and/or revision of the manuscript:** B. Homet Moreno, J.M.  
 591 Zaretsky, J. Tsoi, G. Parisi, A.T. Weeraratna, T.G. Graeber, S. Hu-Lieskovan,  
 592 A. Ribas  
 593 **Administrative, technical, or material support (i.e., reporting or organizing**  
 594 **data, constructing databases):** B. Homet Moreno, J. Tsoi, K. Meeth, A. Ribas  
 595 **Study supervision:** S. Hu-Lieskovan, A. Ribas  
 596 **Other (performed TopFlash Assay and Western blot associated with the**  
 597 **TopFlash Assay):** A. Ndoye

598 **Grant Support**

599 This study was funded in part by the NIH grants P01CA168585 (to A. Ribas  
 600 and T.G. Graeber), R35 CA197633, the Ressler Family Fund, the Dr. Robert  
 601 Vigen Memorial Fund, the Grimaldi Family Fund, the Samuels Family Fund, the  
 602 Ruby Family Fund, the Alexandra Cooper Memorial Fund, and the Garcia-  
 603 Corsini Family Fund (to A. Ribas). B. Homet Moreno was supported in part by  
 604 the Rio Hortega Scholarship (08/142) from the Hospital 12 de Octubre, Madrid,

Spain. G. Parisi was supported in part by the Division of Medical Oncology and  
 Immunotherapy (University Hospital of Siena). J.M. Zaretsky is a member of the  
 UCLA Medical Scientist Training Program supported by NIH NIGMS training  
 grant GM08042. J. Tsoi is supported by the NIH Ruth L. Kirschstein Institutional  
 National Research Service Award#T32-CA009120. S. Hu-Lieskovan was sup-  
 ported by a Young Investigator Award and a Career Development Award from  
 the American Society of Clinical Oncology (ASCO), a Tower Cancer Research  
 Foundation Grant, and a Dr. Charles Coltman Fellowship Award from the Hope  
 Foundation

The costs of publication of this article were defrayed in part by the  
 payment of page charges. This article must therefore be hereby marked  
*advertisement* in accordance with 18 U.S.C. Section 1734 solely to indicate  
 this fact.

Received March 21, 2016; revised July 12, 2016; accepted August 4, 2016;  
 published OnlineFirst xx xx, xxxx.

621 **References**

622 1. Brahmer JR, Tykodi SS, Chow LQ, Hwu WJ, Topalian SL, Hwu P, et al. Safety  
 623 and activity of anti-PD-L1 antibody in patients with advanced cancer.  
 624 *N Engl J Med* 2012;366:2455-65.  
 625 2. Hamid O, Robert C, Daud A, Hodi FS, Hwu WJ, Kefford R, et al. Safety and  
 626 tumor responses with lambrolizumab (anti-PD-1) in melanoma. *N Engl*  
 627 *J Med* 2013;369:134-44.  
 628 3. Ribas A, Schnachter J, V. Long G, Arance A, Grob JJ, Mortier L, et al. Phase III  
 629 study of pembrolizumab (MK-3475) versus ipilimumab in patients with  
 630 ipilimumab-naïve advanced melanoma (abstract CT101). *Am Assoc Can-*  
 631 *cancer Res (Annual Meeting)* 2015.  
 632 4. Topalian SL, Hodi FS, Brahmer JR, Gettinger SN, Smith DC, McDermott DF,  
 633 et al. Safety, activity, and immune correlates of anti-PD-1 antibody in  
 634 cancer. *N Engl J Med* 2012;366:2443-54.  
 635 5. Taube JM, Klein A, Brahmer JR, Xu H, Pan X, Kim JH, et al. Association of  
 636 PD-1, PD-1 ligands, and other features of the tumor immune microenvi-  
 637 ronment with response to anti-PD-1 therapy. *Clin Cancer Res* 2014;20:  
 638 5064-74.  
 639 6. Tumeh PC, Harview CL, Yearley JH, Shintaku IP, Taylor EJ, Robert L, et al.  
 640 PD-1 blockade induces responses by inhibiting adaptive immune resis-  
 641 tance. *Nature* 2014;515:568-71.  
 642 7. Gubin MM, Zhang X, Schuster H, Caron E, Ward JP, Noguchi T, et al.  
 643 Checkpoint blockade cancer immunotherapy targets tumour-specific  
 644 mutant antigens. *Nature* 2014;515:577-81.  
 645 8. Blank C, Kuball J, Voelkl S, Wiendl H, Becker B, Walter B, et al. Blockade of  
 646 PD-L1 (B7-H1) augments human tumor-specific T cell responses in vitro.  
 647 *Int J Cancer* 2006;119:317-27.  
 648 9. Freeman GJ, Long AJ, Iwai Y, Bourque K, Chernova T, Nishimura H, et al.  
 649 Engagement of the PD-1 immunoinhibitory receptor by a novel B7 family  
 650 member leads to negative regulation of lymphocyte activation. *J Exp Med*  
 651 2000;192:1027-34.  
 652 10. Latchman YE, Liang SC, Wu Y, Chernova T, Sobel RA, Klemm M, et al. PD-  
 653 L1-deficient mice show that PD-L1 on T cells, antigen-presenting cells, and  
 654 host tissues negatively regulates T cells. *Proc Natl Acad Sci U S A*  
 655 2004;101:10691-6.  
 656 11. Wang L, Pino-Lagos K, de Vries VC, Guleria I, Sayegh MH, Noelle RJ.  
 657 Programmed death 1 ligand signaling regulates the generation of adaptive  
 658 Foxp3+CD4+ regulatory T cells. *Proc Natl Acad Sci U S A* 2008;105:  
 659 9331-6.  
 660 12. Robert C, Long GV, Brady B, Dutriaux C, Maio M, Mortier L, et al.  
 661 Nivolumab in previously untreated melanoma without BRAF mutation.  
 662 *N Engl J Med* 2015;372:320-30.  
 663 13. Gilchrist BA, Eller MS, Geller AC, Yaar M. The pathogenesis of melanoma  
 664 induced by ultraviolet radiation. *N Engl J Med* 1999;340:1341-8.  
 665 14. Hecht SS. Tobacco smoke carcinogens and lung cancer. *J Natl Cancer Inst*  
 666 1999;91:1194-210.  
 667 15. Carter L, Fouser LA, Jussif J, Fitz L, Deng B, Wood CR, et al. PD-1:PD-L  
 668 inhibitory pathway affects both CD4(+) and CD8(+) T cells and is  
 669 overcome by IL-2. *Eur J Immunol* 2002;32:634-43.  
 670 16. Karwacz K, Arce F, Bricogne C, Kochan G, Escors D. PD-L1 co-stimulation,  
 671 ligand-induced TCR down-modulation and anti-tumor immunotherapy.  
 672 *Oncoimmunology* 2012;1:86-8.

673 17. Karwacz K, Bricogne C, MacDonald D, Arce F, Bennett CL, Collins M, et al.  
 674 PD-L1 co-stimulation contributes to ligand-induced T cell receptor down-  
 675 modulation on CD8+ T cells. *EMBO Mol Med* 2011;3:581-92.  
 676 18. Yokosuka T, Takamatsu M, Kobayashi-Imanishi W, Hashimoto-Tane A,  
 677 Azuma M, Saito T. Programmed cell death 1 forms negative costimulatory  
 678 microclusters that directly inhibit T cell receptor signaling by recruiting  
 679 phosphatase SHP2. *J Exp Med* 2012;209:1201-17.  
 680 19. Harada N, Tamai Y, Ishikawa T, Sauer B, Takaku K, Oshima M, et al.  
 681 Intestinal polyposis in mice with a dominant stable mutation of the beta-  
 682 catenin gene. *EMBO J* 1999;18:5931-42.  
 683 20. McKenna A, Hanna M, Banks E, Sivachenko A, Cibulskis K, Kernytzky A,  
 684 et al. The Genome Analysis Toolkit: A MapReduce framework for analyzing  
 685 next-generation DNA sequencing data. *Genome Res* 2010;20:1297-303.  
 686 21. Shi H, Hugo W, Kong X, Hong A, Koya RC, Moriceau G, et al. Acquired  
 687 resistance and clonal evolution in melanoma during BRAF inhibitor  
 688 therapy. *Cancer Discov* 2014;4:80-93.  
 689 22. Koboldt DC, Zhang Q, Larson DE, Shen D, McLellan MD, Lin L, et al.  
 690 VarScan 2: Somatic mutation and copy number alteration discovery in  
 691 cancer by exome sequencing. *Genome Res* 2012;22:568-76.  
 692 23. McLaren W, Pritchard B, Rios D, Chen Y, Flicek P, Cunningham F. Deriving  
 693 the consequences of genomic variants with the Ensembl API and SNP Effect  
 694 Predictor. *Bioinformatics* 2010;26:2069-70.  
 695 24. Favero F, Joshi T, Marquard AM, Birkbak NJ, Krzystanek M, Li Q, et al.  
 696 Sequenza: Allele-specific copy number and mutation profiles from tumor  
 697 sequencing data. *Ann Oncol* 2015;26:64-70.  
 698 25. Kim D, Pertea G, Trapnell C, Pimentel H, Kelley R, Salzberg SL. TopHat2:  
 699 accurate alignment of transcriptomes in the presence of insertions, dele-  
 700 tions and gene fusions. *Genome Biol* 2013;14:R36.  
 701 26. Trapnell C, Roberts A, Goff L, Pertea G, Kim D, Kelley DR, et al. Differential  
 702 gene and transcript expression analysis of RNA-seq experiments with  
 703 TopHat and Cufflinks. *Nat Protoc* 2012;7:562-78.  
 704 27. Subramanian A, Tamayo P, Mootha VK, Mukherjee S, Ebert BL, Gillette MA,  
 705 et al. Gene set enrichment analysis: A knowledge-based approach for  
 706 interpreting genome-wide expression profiles. *Proc Natl Acad Sci U S A*  
 707 2005;102:15545-50.  
 708 28. Cooper ZA, Juneja VR, Sage PT, Frederick DT, Piris A, Mitra D, et al.  
 709 Response to BRAF inhibition in melanoma is enhanced when combined  
 710 with immune checkpoint blockade. *Cancer Immunol Res* 2014;2:643-54.  
 711 29. Koya RC, Mok S, Comin-Anduix B, Chodon T, Radu CG, Nishimura MI,  
 712 et al. Kinetic phases of distribution and tumor targeting by T cell receptor  
 713 engineered lymphocytes inducing robust antitumor responses. *Proc Natl*  
 714 *Acad Sci U S A* 2010;107:14286-91.  
 715 30. Cross RS, Malaterre J, Davenport AJ, Carpinteri S, Anderson RL, Darcy PK,  
 716 et al. Therapeutic DNA vaccination against colorectal cancer by targeting  
 717 the MYB oncoprotein. *Clin Transl Immunol* 2015;4:e30.  
 718 31. Ngiow SF, Young A, Jacquelot N, Yamazaki T, Enot D, Zitvogel L, et al. A  
 719 threshold level of intratumor CD8+ T-cell PD1 expression dictates ther-  
 720 apeutic response to anti-PD1. *Cancer Res* 2015;75:3800-11.  
 721 32. Mule JJ, Shu S, Schwarz SL, Rosenberg SA. Adoptive immunotherapy of  
 722 established pulmonary metastases with LAK cells and recombinant inter-  
 723 leukin-2. *Science* 1984;225:1487-9.  
 724

- 727 33. Damsky WE, Curley DP, Santhanakrishnan M, Rosenbaum LE, Platt JT, 757  
728 Gould Rothberg BE, et al. Beta-catenin signaling controls metastasis in Braf- 758  
729 activated Pten-deficient melanomas. *Cancer Cell* 2011;20:741–54. 759  
730 34. Spranger S, Bao R, Gajewski TF. Melanoma-intrinsic beta-catenin signalling 760  
731 prevents anti-tumour immunity. *Nature* 2015;523:231–5. 761  
732 35. Ginhoux F, Liu K, Helft J, Bogunovic M, Greter M, Hashimoto D, et al. The 762  
733 origin and development of nonlymphoid tissue CD103+ DCs. *J Exp Med* 763  
734 2009;206:3115–30. 764  
735 36. Ganguly D, Haak S, Sisirak V, Reizis B. The role of dendritic cells in 765  
736 autoimmunity. *Nat Rev Immunol* 2013;13:566–77. 766  
737 37. Ribas A. Adaptive immune resistance: How cancer protects from immune 767  
738 attack. *Cancer Discov* 2015;5:915–9. 768  
739 38. Snyder A, Makarov V, Merghoub T, Yuan J, Zaretsky JM, Desrichard A, et al. 769  
740 Genetic basis for clinical response to CTLA-4 blockade in melanoma. 770  
741 *N Engl J Med* 2014;371:2189–99. 771  
742 39. Rizvi NA, Hellmann MD, Snyder A, Kvistborg P, Makarov V, Havel JJ, et al. 772  
743 Cancer immunology. Mutational landscape determines sensitivity to PD-1 773  
744 blockade in non-small cell lung cancer. *Science* 2015;348:124–8. 774  
745 40. Le DT, Uram JN, Wang H, Bartlett BR, Kemberling H, Eyring AD, et al. PD-1 775  
746 blockade in tumors with mismatch-repair deficiency. *N Engl J Med* 776  
747 2015;372:2509–20. 777  
748 41. Hirano F, Kaneko K, Tamura H, Dong H, Wang S, Ichikawa M, et al. 778  
749 Blockade of B7-H1 and PD-1 by monoclonal antibodies potentiates cancer 779  
750 therapeutic immunity. *Cancer Res* 2005;65:1089–96. 780  
751 42. Escors D, Bricogne C, Arce F, Kochan G, Karwacz K. On the mechanism of T 781  
752 cell receptor down-modulation and its physiological significance. *J Biosci* 782  
753 *Med* 2011;1. 783  
754 43. Konkel JE, Frommer F, Leech MD, Yagita H, Waisman A, Anderton SM. PD- 784  
755 1 signalling in CD4(+) T cells restrains their clonal expansion to an 785  
immunogenic stimulus, but is not critically required for peptide-induced  
tolerance. *Immunology* 2010;130:92–102.  
44. Ueha S, Yokochi S, Ishiwata Y, Ogiwara H, Chand K, Nakajima T, et al.  
Robust antitumor effects of combined anti-CD4-depleting antibody and  
anti-PD-1/PD-L1 immune checkpoint antibody treatment in mice. *Cancer*  
*Immunol Res* 2015;3:631–40.  
45. Gibson A, Ogese M, Sullivan A, Wang E, Saide K, Whitaker P, et al. Negative  
regulation by PD-L1 during drug-specific priming of IL-22-secreting T cells  
and the influence of PD-1 on effector T cell function. *J Immunol*  
2014;192:2611–21.  
46. Pen JJ, Keersmaecker BD, Heirman C, Corthals J, Liechtenstein T, Escors D,  
et al. Interference with PD-L1/PD-1 co-stimulation during antigen presen-  
tation enhances the multifunctionality of antigen-specific T cells. *Gene*  
*Ther* 2014;21:262–71.  
47. Blank C, Gajewski TF, Mackensen A. Interaction of PD-L1 on tumor cells  
with PD-1 on tumor-specific T cells as a mechanism of immune evasion:  
Implications for tumor immunotherapy. *Cancer Immunol Immunother*  
2005;54:307–14.  
48. Sanchez-Paulete AR, Cueto FJ, Martinez-Lopez M, Labiano S, Morales-  
Kastresana A, Rodríguez-Ruiz ME, et al. Cancer immunotherapy with  
immunomodulatory anti-CD137 and anti-PD-1 monoclonal antio-  
dies requires BATF3-dependent dendritic cells. *Cancer Discov* 2016;6:  
71–9.  
49. Harlin H, Meng Y, Peterson AC, Zha Y, Tretiakova M, Slingluff C, et al.  
Chemokine expression in melanoma metastases associated with CD8+  
T-cell recruitment. *Cancer Res* 2009;69:3077–85.  
50. Peng W, Liu C, Xu C, Lou Y, Chen J, Yang Y, et al. PD-1 blockade enhances T-  
cell migration to tumors by elevating IFN-gamma inducible chemokines.  
*Cancer Res* 2012;72:5209–18.



## AUTHOR QUERIES

### AUTHOR PLEASE ANSWER ALL QUERIES

- Q1: Page: 1: AU: Per journal style, genes, alleles, loci, and oncogenes are italicized; proteins are roman. Please check throughout to see that the words are styled correctly. AACR journals have developed explicit instructions about reporting results from experiments involving the use of animal models as well as the use of approved gene and protein nomenclature at their first mention in the manuscript. Please review the instructions at <http://www.aacrjournals.org/site/InstrAuthors/ifora.xhtml#genomen> to ensure that your article is in compliance. If your article is not in compliance, please make the appropriate changes in your proof.
- Q2: Page: 1: Author: Please verify the drug names and their dosages used in the article.
- Q3: Page: 1: Author: Please check the affiliation addresses as set for correctness.
- Q4: Page: 1: Author: Please verify the affiliations and their corresponding author links.
- Q5: Page: 1: Author: Please verify the corresponding author details.
- Q6: Page: 2: Author: Please define "AALAC."
- Q7: Page: 2: Author: Units of measurement have been changed here and elsewhere in the text from "M" to "mol/L," and related units, such as "mmol/L" and " $\mu$ mol/L," in figures, legends, and tables in accordance with journal style, derived from the Council of Science Editors Manual for Authors, Editors, and Publishers and the Système international d'unités. Please note if these changes are not acceptable or appropriate in this instance.
- Q8: Page: 2: Author: Please check "ratio.priority" for sense.
- Q9: Page: 2: Author: Please define "OCT."
- Q10: Page: 3: Author: Please confirm quality/labeling of all images included within this article. Thank you.
- Q11: Page: 6: Author: Please verify the reference to "2C" in the part "analysis of the 2C total number" for sense.
- Q12: Page: 6: Author: Please define "APCs."
- Q13: Page: 11: AU:/PE: The conflict-of-interest disclosure statement that appears in the proof incorporates the information from forms completed and signed off on by each individual author. No factual changes can be made to disclosure information at the proof stage. However, typographical errors or misspelling of author names should be noted on the proof and will be corrected before publication. Please note if any such errors need to be corrected. Is the disclosure statement correct?
- Q14: Page: 12: Author: The contribution(s) of each author are listed in the proof under the heading "Authors' Contributions." These contributions are derived from forms completed and signed off on by each individual author. As the corresponding author, you are

permitted to make changes to your own contributions. However, because all authors submit their contributions individually, you are not permitted to make changes in the contributions listed for any other authors. If you feel strongly that an error is being made, then you may ask the author or authors in question to contact us about making the changes. Please note, however, that the manuscript would be held from further processing until this issue is resolved.

Q15: Page: 12: Author: Please verify the heading "Grant Support" and its content for correctness.

Q16: Page: 12: Author: Ref. 37 has been updated as per PubMed. Please verify.

Q17: Page: 12: Author: Please provide volume and page range for ref. 3.

AU: Below is a summary of the name segmentation for the authors according to our records. The First Name and the Surname data will be provided to PubMed when the article is indexed for searching. Please check each name carefully and verify that the First Name and Surname are correct. If a name is not segmented correctly, please write the correct First Name and Surname on this page and return it with your proofs. If no changes are made to this list, we will assume that the names are segmented correctly, and the names will be indexed as is by PubMed and other indexing services.

<b>First Name</b>	<b>Surname</b>	<b>Antoni</b>	<b>Ribas</b>
Blanca			
Homet Moreno			
Jesse M.	Zaretsky		
Angel	Garcia-Diaz		
Jennifer	Tsoi		
Giulia	Parisi		
Lidia	Robert		
Katrina	Meeth		
Abibatou	Ndoye		
Marcus	Bosenberg		
Ashani T.	Weeraratna		
Thomas G.	Graeber		
Begoña	Comin-Anduix		
Siwen	Hu-Lieskovan		